RSC Advances

ROYAL SOCIETY OF CHEMISTRY

www.rsc.org/advances

Journal Name

RSCPublishing

COMMUNICATION

Monolayer Graphene-supported Free-standing PS-*b*-PMMA Thin Film with Perpendicularly Orientated Microdomains

Cite this: DOI: 10.1039/x0xx00000x

Received 00th January 2012,
Accepted 00th January 2012

DOI: 10.1039/x0xx00000x

www.rsc.org/

Mei-Ling Wu,[ab] Jing Li,[ab] Li-Jun Wan,[a] and Dong Wang*[a]

A facile way to fabricate robust free-standing BCP thin films with perpendicularly orientated microdomains on CVD-grown monolayer graphene support is reported. Graphene plays as both the neutral surface to control the assembly of BCP film and the support of the thin film to provide high mechanical strength. The free-standing BCP films with nanopattern can be used as a substrate-independent template to facilitate BCP nano-lithography.

During the past few decades, block copolymer (BCP) thin film based nanopatterning techniques have attracted enormous attention.[1, 2] The self-assembly of BCPs, which is driven by the microphase separation of polymer blocks with different properties, can lead to various ordered nanostructures, and act as templates to control the spatial order of other matters. The combined features such as tunable nano-scale feature size,[3] designable pattern symmetry,[4] high throughput,[5] great compatibility with the current top-down patterning techniques, make BCP-based patterning techniques a promising solution for the further microelectronic device miniaturization.[6, 7] In addition, the applications of BCP patterning techniques for magnetic storage devices,[8] photovoltaic devices,[9] microreactors,[10] and porous filtration membranes have been well-demonstrated.[11]

In a typical BCP lithography process, the controllable formation of perpendicularly oriented microdomains in BCP thin film is a crucial step to facilitate pattern transfer.[12, 13] The strategy of surface modification of the substrate to obtain "neutral" surface for two immiscible blocks is widely applied to achieve perpendicular orientation.[14-16] Nowadays some methods of surface modification to control the microdomain orientation have been developed,[17] yet most of them are subject to specific substrate and/or tedious preparation steps.[18, 19] In this regard, free-standing BCP thin films is highly desirable as a universal substrate-independent template for nanopattern technology,[20, 21] as it can be transferred onto arbitrary substrate, including rough surface, flexible substrate, substrate with low surface energy, and heat-labile substrate.[22] Unfortunately, although there are a few reported methods to prepare free-standing polymer films by floating films off the substrate,[23] the resulting thin films are not robust enough to keep the BCP nanopatterns intact, and are generally used for characterization only.[24, 25] Gopalan et al recently develop a pre-assembled BCP thin film that can be transferred onto Cu foil or graphene/Cu substrate.[26] The transferrable BCP films show importance in nanopattern technology, but for more versatile applications, we aspire for free-standing BCP thin films with higher quality and better mechanical strength.

Previously, BCP nanolithography technique has been used to pattern graphene to tune the electronic properties of graphene-related materials.[27, 28] In these works, the graphene is just used as the substrate to be etched, not for free-standing BCP films. Recently, Kim et al show that transferable BCP nanopatterns can be assembled on modified graphene films using spin-coated reduced graphene oxide as the substrate.[22, 29] However, the thermal or chemical reduced graphene films are obtained from small-flake graphene oxide and therefore have less uniform film thickness and integrity.[30] Compared with the reduced graphene, graphene grown by chemical vapor deposition (CVD) holds several intrinsic advantages, such as large area, high quality, controllable layers, and unambiguous thickness.[31, 32] Particularly, the monolayer graphene shows superb mechanical properties, with intrinsic strength of 130 GPa and a Young's modulus of 1 TPa, exceeding any other materials.[33, 34] The monolayer graphene promises ideal support for robust free-standing BCP films. Herein, we adopt CVD-grown monolayer graphene as a thin but robust support for the fragile BCP thin films. Although pristine graphene is hydrophobic with low surface energy, its surface energy is tunable.[35, 36] Via a mild UV/ozone (UVO) based protocol to tune the surface energy of the graphenes, we demonstrate that free-standing PS-*b*-PMMA thin films with perpendicularly orientated microdomains can be fabricated on graphene. The free-standing films show satisfactory mechanical strength, and thus can be transferred and applied as the nanopattern template for other applications.

The overall fabrication process for the free-standing BCP films on graphene with perpendicularly orientated morphology is schematically illustrated in Fig. 1. Graphene grown by CVD on copper foil is used as the support for BCP thin film. First, we control the wetting property of graphene by UVO treatment, which is a simple, mild, and controllable oxidation method for graphene.[37] Next, cylinder-forming or lamella-forming PS-*b*-PMMAs, determined by the volume fraction of the BCP blocks,

are spin-coated onto the modified graphene. BCP films with perpendicular orientation morphology are afforded after a proper thermal annealing process to induce the microphase separation. Finally, the well-developed technique of graphene transfer is borrowed to fabricate free-standing PS-*b*-PMMA thin films on graphene simply by etching the Cu foil. The overall process for free-standing BCP film is simple and straightforward, effectively preserving the BCP nanopattern.

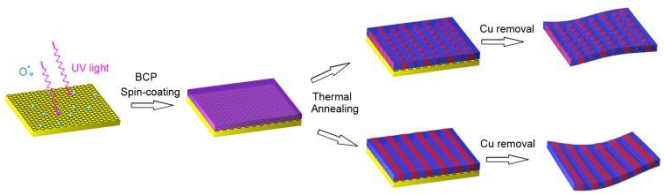

Fig. 1 Schematic procedure of producing free-standing PS-*b*-PMMA thin films with perpendicular orientation of microdomains on monolayer graphene treated by UVO.

The morphology of BCP films is governed by the interfacial energy/interaction between the BCP and the substrate. The pristine graphene has low surface energy and good affinity to the PS blocks. With UVO treating, graphenes with different oxidation degree and thus different interfacial energy are obtained. Raman and X-ray photoelectron spectroscopy (XPS) are employed to track the evolution of the structural and chemical information of the graphene films with UVO treatment. The intensity ratio between 2D (~2680 cm^{-1}) and G (~1580 cm^{-1}) band (I_{2D}/I_G) gradually decreases with exposure time, and the 2D and G peaks become broad (Fig. 2a). In addition, the intensity ratio between D (~1350 cm^{-1}) and G band (I_D/I_G) increases dramatically and finally stabilizes to ~1, exhibiting a two-step evolution.[38] According to XPS results (Fig. 2b), after graphene is exposed to UVO for 7 min, C=O bond (290.0 eV) appears and the relative intensity of C-O bond (286.4 eV) increases. Raman and XPS results verify that the graphenes are gradually oxidized by UVO exposure. Evolution of the static water contact angle (θ_w) of the graphene films further shows that θ_w gradually decreases from the pristine 83.6 ° to 68.5 ° with exposure time of 15 min (Fig. 2c). This indicates that with the oxidization by UVO, the graphene carries more polar groups, presumably O-containing functional groups, becoming more hydrophilic. The surface energies of graphene films exposed to UVO for 5 min and 7 min, measured according to Neumann's method (detailed data in Table S1, ESI †),[39] are (59.0 ±0.4) mJ/m^2 and (60.1 ±0.3) mJ/m^2, respectively. The surface energies are between that of graphene and graphene oxide, indicating that the treated graphene films are oxidized to a proper degree.[40]

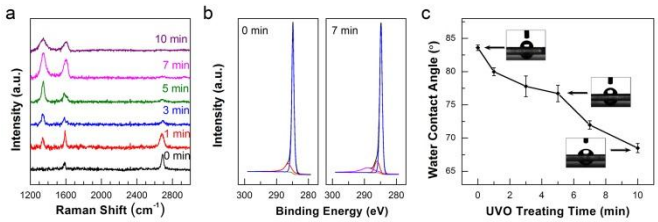

Fig. 2 (a) Raman spectra of CVD-grown graphene films exposed to UVO for different time; (b) XPS spectra of the graphene before and after UVO treatment; (c) water contact angles of the graphene films with various UVO treating time (typical photographs of water drops are shown as insets).

The modified graphenes with tunable surface tension/energy are applied to manipulate the morphology of the BCP films. Fig. 3 displays the scanning electron microscopy (SEM) images of the morphology of the cylinder-forming (a–e) and lamella-forming (f–j) PS-*b*-PMMA on graphenes that have been treated by UVO with varied time. For the cylinder-forming PS-*b*-PMMA films (Fig. 3a–e), the perpendicularly and parallelly oriented morphology present as hexagonal array and fingerprint array, respectively; for the lamella-forming PS-*b*-PMMA films (Fig. 3f–j), the fingerprint array and featureless morphology are ascribed to the perpendicularly and parallelly oriented morphology. We have carried out a statistical analysis of p_p (the areal percentage of perpendicularly oriented domains in the whole BCP film) to understand the evolution of BCP morphology on wetting property of UVO-treated graphene (Fig. S1, ESI†). For the cylinder-forming films, we can see that on the pristine graphene, parallel orientation of microdomains is dominated, covering almost the whole area of the BCP film (Fig. 3a). With the UVO treating time increased, p_p increases from ~59.0% at 3 min to ~95.6% at 7 min with highly ordered cylinder morphology (Fig. 3b–d). With the UVO treating time further increased to 10 min, however, only sparse features of perpendicularly orientated microdomains are observed (Fig. 3e). For the lamella-forming PS-*b*-PMMA film, the evolution tendency of p_p upon UVO treating time of underlying graphenes is similar with the cylinder one. The portion of the fingerprint morphology increases gradually with the oxidization degree of graphenes (i.e. the UVO treating time, Figure 3f–i), and decreases abruptly at 10 min, which is excessively oxidized (Fig. 3j). The variation of the BCP morphology is considered as a result of the interface energy (E_i) of graphene.[19, 29] By controlling the E_i of graphene with UVO treatment, we are able to control the perpendicular orientation of microdomains in BCP thin films conveniently. Intriguingly, Kim et al prove that graphene oxide can also be reduced to a suitable E_i to be a neutralized surface to induce BCP morphology. In conjunction with their results, our results help to comprehensively reveal the effect of E_i of substrates, from graphene to graphene oxide, on the morphology of BCP self-assembly. BCP film on the graphene treated for 7 min exhibits the highest p_p, and is adopted as the optimal condition in the following experiment.

In addition to the interfacial energy/tension, the thickness of BCP films is also an important parameter affecting the morphology. The film thickness window of the cylinder-forming PS-*b*-PMMA film, in which the structure of perpendicularly oriented microdomain persists, is 30.0–89.0 nm on graphenes (Fig. S2, ESI†). This thickness dependence of the perpendicular orientation microdomains results from the boundary conditions of substrate and free surface (see Fig. S2, ESI† for more discussion). The wide thickness window offers more choices of film thickness.

Based on the optimum condition of pattern control, we are able to get a large-areal nanopattern on the whole copper foil (cm-scale). Upon formation, free-standing BCP films on graphenes can be obtained by etching the Cu substrate in saturated $(NH_4)_2S_2O_8$ solution for a short time (Fig. S3a, ESI†). Owing to the beneficial mechanical property of underlying graphene, the large-areal free-standing film with nanopattern is easy to transfer to various substrates, such as solid substrates (ITO and Si), and even flexible and thermal/chemical instable substrates such as polydimethylsiloxane (PDMS) and poly-ethylene terephthalate (PET) (Fig. S3, S4, ESI†). It is noteworthy that the conventional method of interfacial wettability controlled by P(S-*r*-MMA) is hardly applicable for

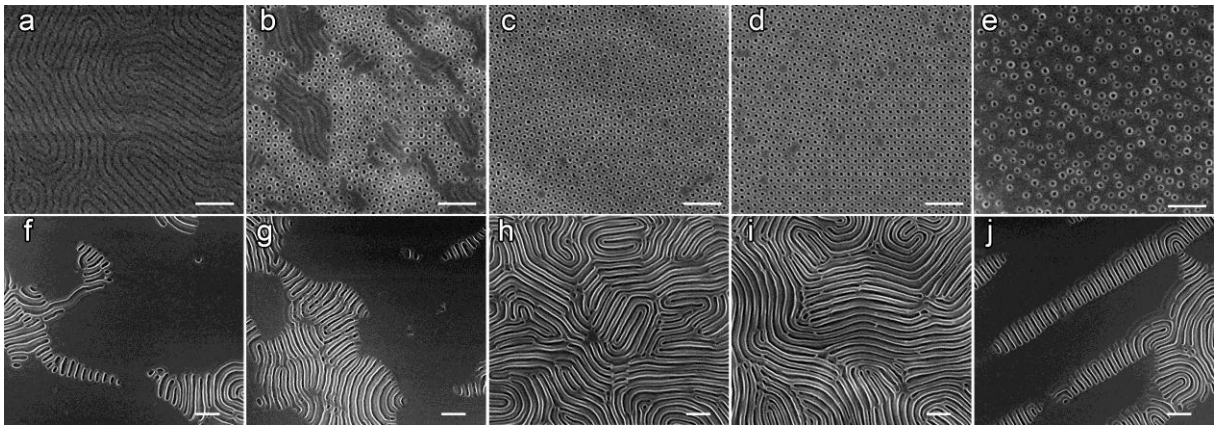

Fig. 3. SEM images of the (a–e) cylinder-forming (58.8 nm) and (f–j) lamella-forming (77.5 nm) PS-*b*-PMMAs self-assembled on graphene films exposed to UVO for various time: (a, f) 0 min, (b, g) 3 min, (c, h) 5 min, (d, i) 7 min, and (e, j) 10 min (scale bar: 200 nm).

PDMS and PET. Also, because of the graphene underneath the BCP film (Fig. S5a, ESI†), the BCP pattern is robust and stays intact even if folded (Fig. S5b, ESI†). BCP nanopattern alone can hardly survive from such deformation without graphene.

As one of many possible subsequent patterning applications of the free-standing BCP film, we show the patterned deposition of Au nanoparticles using the BCP template. The procedure is illustrated in Fig. 4a. First, a free-standing lamellar-forming PS-*b*-PMMA film with uniform fingerprint morphology on graphene is transferred onto Si wafer (Figure 4b). Next, the PMMA blocks and the graphene beneath are removed with brief Ar plasma exposure to form a PS template. Au nanoparticles are then deposited on Si substrate via galvanic displacement.[41] Since Au particle deposition can only occur where PMMA and graphene are removed and the silicon is exposed to the solution, Au nanoparticles are deposited in the intervals of PS template (Fig. 4c). From the side view SEM image, we can clearly see both Au nanoparticles and PS template (inset in Fig. 4c). Au nanoparticles deposited precisely in the intervals of PS indicate a conformal and defect-free contact between BCP-graphene films and substrate. If otherwise, Au nanoparticles would deposit randomly between the film and substrate or in the defect region and thus cannot form the patterns. As the interaction between graphene and Si wafer is weak, the template can be completely peeled off with adhesive tape in a simple way. After that, Au nanoparticle pattern replicating the PMMA pattern is obtained (Fig. 4d). PS and graphene are no longer observed from the side view (inset in Fig. 4d). This easy removal of the template can be also demonstrated by Raman spectra (Fig. 4e). The Raman signals of graphenes and the PS blocks (Fig. S6, ESI†) can be seen before peeling off and are enhanced upon deposition of Au (due to the surface enhanced Raman scattering effect).[37] After peeling off PS blocks and graphene, these signals disappear, indicating a complete removal. The compatibility of the graphene-supported BCP films with even solution-phase reaction indicates that free-standing BCP films can form conformal and defect-free contact upon transferring to other substrate. On the other hand, the capability to be easily peeled off after pattern transfer is another benign feature. These features are resulted from the high integrity and superb mechanical property of the graphene supports, which also demonstrate the advantages of free-standing BCP film on monolayer graphene.

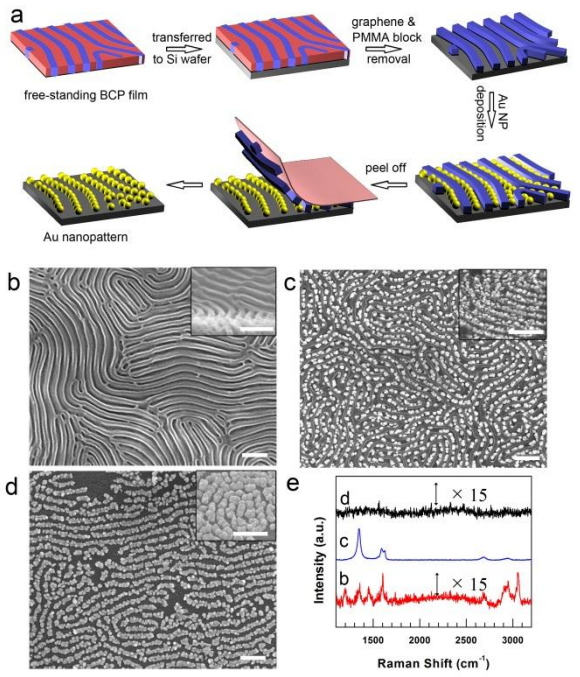

Fig. 4. (a) Schematic procedure of Au nanopattern formation using the free-standing PS-*b*-PMMA film; SEM images of (b) the lamellar-forming PS-*b*-PMMA film (77.5 nm in thickness) on the graphene films exposed to UVO for 7 min, which is transferred onto Si wafer, (c) Au nanopattern formed in the intervals of PS block, and (d) Au nanopattern with the template removed; (insets showing the corresponding side view, scale bar: 200 nm) (e) Raman spectra of the samples in b, c, and d.

In summary, we have demonstrated a simple yet effective way to form free-standing PS-*b*-PMMA thin films with perpendicular microdomain orientation using CVD-grown monolayer graphene as support. By controlling the UVO treating time, we tune the surface energy of graphene and achieve a highly ordered and perpendicular microdomain orientation of BCP film with large size. Benefited from the support of monolayer graphene, the free-standing PS-*b*-PMMA thin film holds unique advantages. (1) Graphene plays as support as well as neutralized surface. Large-sized PS-*b*-PMMA thin film with nanopatterns can be self-assembled simply by tuning the surface energy of graphene on Cu foil.

The straightforward method greatly simplifies the preparation process and avoids possible damage to BCP nanopattern. (2) Monolayer graphene provides strong support for the BCP pattern, resulting in a free-standing BCP film with satisfactory mechanical properties. The robust free-standing thin film is independent of the substrate and is thus feasible to be transferred to many substrates, including flexible and thermal/chemical instable substrates, for further nanopatterning. (3) The CVD-grown graphene has high quality and integrity, which promises BCP nanopattern with few defects. It also has controllable and homogenous layers/thickness, which greatly facilitates the processing during BCP lithography. (4) BCP nanopattern fabricated on monolayer graphene also provides convenience for nanopattern of integrated graphene, which will promise potential applications in semiconductor devices and nanoelectronic field.

This work was supported by the National Key Project on Basic Research (Grants 2011CB808700, 2011CB932300), National Natural Science Foundation of China (21121063, 21127901), and the Strategic Priority Research Program of the Chinese Academy of Sciences (Grant No. XDB12020100).

Notes and references

[a] Kay Laboratory of Molecular Nanostructure and Nanotechnology and Beijing National Laboratory for Molecular Sciences, Institute of Chemistry, Chinese Academy of Sciences (CAS), Beijing 100190, P. R. China. E-mail: wangd@iccas.ac.cn

[b] University of CAS, Beijing 100049, P. R. China

†Electronic Supplementary Information (ESI) available: Experimental details and additional figures. See DOI: 10.1039/c000000x/

1. C. T. Black, R. Ruiz, G. Breyta, J. Y. Cheng, M. E. Colburn, K. W. Guarini, H. C. Kim and Y. Zhang, *IBM J. Res. Dev.*, 2007, **51**, 605-633.
2. Y.-C. Tseng and S. B. Darling, *Polymers*, 2010, **2**, 470-489.
3. S. Kim, P. F. Nealey and F. S. Bates, *Nano Lett.*, 2014, **14**, 148-152.
4. H. Yi, X. Y. Bao, J. Zhang, C. Bencher, L. W. Chang, X. Chen, R. Tiberio, J. Conway, H. Dai, Y. Chen, S. Mitra and H. S. Wong, *Adv. Mater.*, 2012, **24**, 3107-3114.
5. M. S. Onses, C. Song, L. Williamson, E. Sutanto, P. M. Ferreira, A. G. Alleyne, P. F. Nealey, H. Ahn and J. A. Rogers, *Nat. Nanotechnol.*, 2013, **8**, 667-675.
6. J. Chai, D. Wang, X. Fan and J. M. Buriak, *Nat. Nanotechnol.*, 2007, **2**, 500-506.
7. S. Park, D. H. Lee, B. Kim, S. W. Hong, U. Jeong, T. Xu and T. P. Russell, *Science*, 2009, **323**, 1030-1033.
8. K. Naito, H. Hieda, M. Sakurai, Y. Kamata and K. Asakawa, *IEEE Trans. Magn.*, 2002, **38**, 1949-1951.
9. B. Hua, Q. Lin, Q. Zhang and Z. Fan, *Nanoscale*, 2013, **5**, 6627-6640.
10. X. Deng, J. M. Buriak, P. X. Dai, L. J. Wan and D. Wang, *Chem. Commun.*, 2012, **48**, 9741-9743.
11. S. Y. Yang, I. Ryu, H. Y. Kim, J. K. Kim, S. K. Jang and T. P. Russell, *Adv. Mater.*, 2006, **18**, 709-712.
12. C. M. Bates, M. J. Maher, D. W. Janes, C. J. Ellison and C. G. Willson, *Macromolecules*, 2014, **47**, 2-12.
13. Y. Qiao, D. Wang and J. M. Buriak, *Nano Lett.*, 2007, **7**, 464-469.
14. P. Mansky, Y. Liu, E. Huang, T.P.Russell and C. Hawker, *Science*, 1997, **275**, 1458-1460.
15. D. Y. Ryu, K. Shin, E. Drockenmuller, C. J. Hawker and T. P. Russell, *Science*, 2005, **308**, 236-239.
16. C. M. Bates, T. Seshimo, M. J. Maher, W. J. Durand, J. D. Cushen, L. M. Dean, G. Blachut, C. J. Ellison and C. G. Willson, *Science*, 2012, **338**, 775-779.
17. B. H. Kim, D. H. Lee, J. Y. Kim, D. O. Shin, H. Y. Jeong, S. Hong, J. M. Yun, C. M. Koo, H. Lee and S. O. Kim, *Adv. Mater.*, 2011, **23**, 5618-5622.
18. J. N. Albert, M. J. Baney, C. M. Stafford, J. Y. Kelly and T. H. Epps, *ACS nano*, 2009, **3**, 3977-3986.
19. E. Han, K. O. Stuen, M. Leolukman, C.-C. Liu, P. F. Nealey and P. Gopalan, *Macromolecules*, 2009, **42**, 4896-4901.
20. D. Feng, Y. Lv, Z. Wu, Y. Dou, L. Han, Z. Sun, Y. Xia, G. Zheng and D. Zhao, *J. Am. Chem. Soc.*, 2011, **133**, 15148-15156.
21. D. Wang and L. Liu, *Chem. Mater.*, 2010, **22**, 6656-6664.
22. J. Kim, B. Kim, J. Hwang, S.-J. Jeong, D. Shin, J. Mun, Y. Choi, H. Jin and S. Kim, *Adv. Mater.*, 2013, **25**, 1331-1335.
23. H. B. Salmaan, S. Michael, A.-R. Chantel, J. N. Art, C. Maverick, L. Shuali, Y. Kelly and I. S. Tayyab, *Langmuir*, 2014, **30**, 5126-5132.
24. B.-H. Sohn, S.-I. Yoo, B.-W. Seo, S.-H. Yun and S.-M. Park, *J. Am. Chem. Soc.*, 2001, **123**, 12734-12735.
25. Q. Zhang, S. Gupta, T. Emrick and T. P. Russell, *J. Am. Chem. Soc.*, 2006, **128**, 3898-3899.
26. J. W. Choi, M. Kim, N. S. Safron, M. S. Arnold and P. Gopalan, *ACS Appl. Mater. Interfaces*, 2014, **6**, 9442-9448.
27. J. Bai, X. Zhong, S. Jiang, Y. Huang and X. Duan, *Nat. Nanotechnol.*, 2010, **5**, 190-194.
28. X. Liang and S. Wi, *ACS nano*, 2012, **6**, 9700-9710.
29. B. H. Kim, J. Y. Kim, S. J. Jeong, J. O. Hwang, D. H. Lee, D. O. Shin, S. Y. Choi and S. O. Kim, *ACS nano*, 2010, **4**, 5464-5470.
30. J. T. Robinson, M. Zalalutidinov, J. W. Baldwin, E. S. Snow, Z. Wei, P. Sheehan and B. H. Houston, *Nano Lett.*, 2008, **8**, 3441-3445.
31. X. Li, W. Cai, J. An, S. Kim, J. Nah, D. Yang, R. Piner, A. Velamakanni, I. Jung, E. Tutuc, S. K. Banerjee, L. Colombo and R. S. Ruoff, *Science*, 2009, **324**, 1312-1314.
32. J. Li, H. Ji, X. Zhang, X. Wang, Z. Jin, D. Wang and L.-J. Wan, *Chem. Commun.*, 2014, **50**, 11012-11015.
33. K. S. Novoselov, A. K. Geim, S. V. Morozov, D. Jiang, Y. Zhang, S. V. Dubonos, I. V. Grigorieva and A. A. Firsov, *Science*, 2004, **306**, 666-669.
34. C. Lee, X. Wei, J. W. Kysar and J. Hone, *Science*, 2008, **321**, 385-388.
35. Z. Chen, L. Dong, D. Yang and H. Lu, *Adv. Mater.*, 2013, **25**, 5352-5359.
36. A. Checco, A. Rahman and C. T. Black, *Adv. Mater.*, 2014, **26**, 886-891.
37. S. Huh, J. Park, Y. S. Kim, K. S. Kim, B. H. Hong and J. M. Nam, *ACS nano*, 2011, **5**, 9799-9806.
38. A. Eckmann, A. Felten, A. Mishchenko, L. Britnell, R. Krupke, K. S. Novoselov and C. Casiraghi, *Nano Lett.*, 2012, **12**, 3925-3930.
39. D. Li and A. Neumann, *J. Colloid Interface Sci.*, 1992, **148**, 190-200.
40. S. Wang, Y. Zhang, N. Abidi and L. Cabrales, *Langmuir*, 2009, **25**, 11078-11081.
41. S. Y. Sayed, F. Wang, M. Malac, A. Meldrum, R. F. Egerton and J. M. Buriak, *ACS nano*, 2009, **3**, 2809-2817.

For Table of Contents only

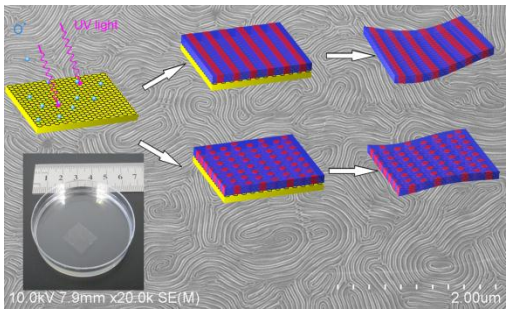

A facile way to fabricate robust free-standing PS-*b*-PMMA thin films with perpendicularly orientated microdomains on monolayer graphene is reported.

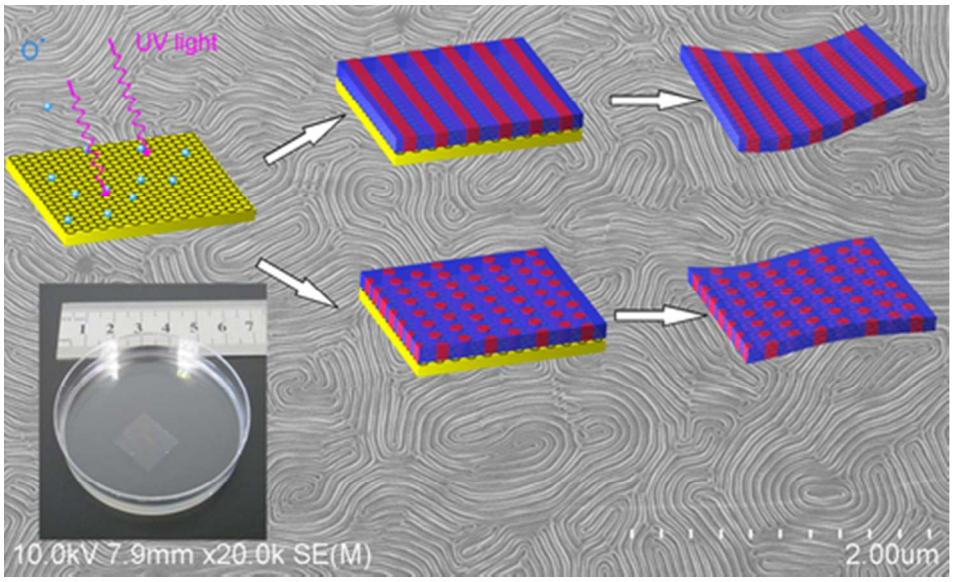

39x24mm (300 x 300 DPI)